Electrochemical Materials and Technologies

REVIEW

Electrochemical Materials and Technologies

eISSN: 2949-0561

Cite this: Electrochem. Mater. Technol. 4 (2025) 20254049

Thermal expansion of alkali and alkaline earth halides in solid and molten states

Olga Tkacheva [a] *

Received: 12 February 2025
Accepted: 12 March 2025
Published online: 18 March 2025

DOI: 10.15826/elmattech.2025.4.049

Thermophysical properties of the alkali and alkaline earth halides, widely used in numerous electrochemical technological processes, are necessary for the design and operation of various devices in a wide temperature range. This review discusses the thermal expansion coefficients of solid and molten salts of the alkali and alkaline earth fluorides and chlorides, the regularities of their change depending on the nature, molar volume and temperature. The thermal expansion of the solid alkali and alkaline earth halides in the range from room temperature to the melting point does not obey a linear law. When salts melt, the thermal expansion coefficient increases, and the increase is greater the larger the cation size. In the liquid state, the temperature dependence of the volumetric thermal expansion coefficient is linear and changes slightly with temperature. The dependence of the thermal expansion of all molten alkali halides on the molar volume can be described by a linear function, which indicates the uniformity of interparticle interactions in these salts and the ionic nature of the bond. For fluorides and chlorides of alkaline earth metals, such a dependence is more complex.

keywords: alkali and alkaline earth halides, thermal expansion coefficient, melt, solid, molar volume

1. Introduction

Both molten and solid salts of the alkali and alkaline earth fluorides and chlorides are widely used in various fields of research and technology. Solid halides can be employed as heat-storing materials or electrolytes for chemical current sources [1, 2]. Nowadays, the halide solid-state electrolytes have received new development for all-solid-state batteries, since, compared to other electrolytes (oxide, sulfide), they have more balanced properties in various aspects, including ionic conductivity, electrochemical stability window, and moisture resistance [3]. Thermal energy accumulation can be carried out as latent accumulation due to various phase transitions, of which in the practice of heat accumulation (heat engineering and heat power engineering) the most common type of phase transformation is the "solid – liquid" transition [4].

The most common area of application of molten halide salts as a medium for technological processes is electrolysis, which is utilized to produce light metals such as aluminum, magnesium, calcium, alkali metals, etc. [5–7]. The production and refining of heavy, rare and refractory metals is effectively carried out in molten salts [8]. In recent years, a new direction in the application of molten salts has been actively developing, associated with the creation of molten salt nuclear reactors. In particular, the process of reprocessing spent nuclear fuel with a high burnup rate for fast neutron reactors requires the creation of new technologies. Molten salt nuclear reactors designed for the transmutation of minor actinides involve the use of molten halide mixtures as a fuel salt or a coolant [9–11]. Galvanoplastic coatings of metals and alloys in halide molten salts play an important role in engineering and industry [12, 13]. The use of such materials increases the efficiency and durability of equipment, reduces the costs of maintenance and repair of structures, and provides a higher level of safety and reliability.

The wide involvement of molten halide salts in technological processes is due to the successful

a: Laboratory of Electrode Processes and Galvanotechnics, Institute of High Temperature Electrochemistry, Ural Branch of the Russian Academy of Sciences Ekaterinburg 620066, Russia

* Corresponding author: o.tkacheva@ihte.ru

combination of their physical and chemical properties: high electrical conductivity, low viscosity, thermal stability, and relatively low volatility. Technological processes are usually carried out at operating temperatures close to the liquidus temperature of salt systems. This means that there is a high probability of solid phase formation in the event of some operational disturbances or, conversely, special targeted deposition (side ledge, crust) is carried out, for example, on the walls of an electrolysis bath, as occurs when starting an aluminum cell [14, 15]. In some cases, the electrolytic production of coatings is carried out in molten salts at temperatures below the melting point of the component being deposited [16].

Thus, many chemical and electrochemical processes involving alkali and alkaline earth halides are accompanied by liquid-solid phase transitions, which dramatically affect the change in the physicochemical properties of salt systems. The coefficient of thermal expansion (CTE) refers to such parameters. The values of CTE and the patterns of their change in solid and liquid states differ significantly, which must be taken into account when solving scientific and engineering issues related to both the development of new technologies and the design and calculation of critical and science-intensive parts and units of electrochemical devices and apparatuses operating in a wide temperature range. Knowledge of the CTE is necessary not only for design calculations of equipment, but also as a unique property of each material for studying the structure, strength of chemical bonds, etc.

The objective of this work is to generalize the available literature data related to the thermal expansion of alkali and alkaline earth halides in solid and molten states.

When a substance (body) is heated, the kinetic energy of the atoms increases, leading to a growth in their natural vibration, which counteracts intermolecular forces and promotes the removal of atoms or molecules from each other, while the size of the body increases. The amount by which a substance expands in response to an increase in temperature is mathematically expressed by the coefficient of thermal expansion (CTE). The higher the CTE of a material the more it will expand in response to heating.

Crystals tend to have the lowest CTEs because their structure is extremely homogeneous and strong. For example, diamond has the lowest known coefficient of thermal expansion of all naturally occurring materials ($1.1 \cdot 10^{-6}$ K^{-1}) [17]. Solids with the highest CTEs have weak intermolecular bonds (usually polymers). For example, the CTE of polyvinylidene fluoride (PVDF) is $1.28 \cdot 10^{-4}$ K^{-1}. Metals tend to have relatively low coefficients (the CTE of iron is $1.13 \cdot 10^{-5}$ K^{-1} [18]), but they have high melting points and are not susceptible to expansion stress-induced failure. This makes metals ideal candidates for use as structural materials in thermal expansion measurements [19].

Some materials exhibit not expansion but, on the contrary, compression with increasing temperature, i.e. they have a negative CTE. This phenomenon has been found for ceramic systems, for example, $LiAlSiO_4$, $Li_2Al_2O_4 \cdot nSiO_2$, ZrW_2O_6 [20, 21]. They have a crystallographic cubic structure, but an isotropic change in interatomic distances with increasing temperature. There are also some metals and alloys that are characterized by low, zero or negative thermal expansion [22]. For example, the $Fe_{65}Ni_{35}$ alloy changes from a paramagnet to a ferromagnet when cooled, and at room temperature its CTE is almost zero.

A distinction is made between the coefficients of volumetric (β) and linear (α) thermal expansion. Gases and liquids always expand within the volumes of their vessels, so they are characterized by the coefficient of volumetric thermal expansion. The relative change in the volume of a body (V) that occurs as a result of a change in its temperature by 1 degree at constant pressure is described by the equation:

$$\beta = 1/V \cdot (\partial V/\partial T)_P. \quad (1)$$

The length of a body can be measured much more accurately than its volume, so it is common to measure the change in the linear dimensions of a solid body caused by a change in temperature. The relative change in the linear dimensions of the body (L) that occurs as a result of the change in its temperature by 1 degree at constant pressure is described by the equation:

$$\alpha = 1/L \cdot (\partial L/\partial T)_P \approx \Delta L/(L \cdot \Delta T). \quad (2)$$

In general, the α may be varied when measured along different directions. For example, for anisotropic crystals, the coefficients of linear expansion along three perpendicular axes are different. For amorphous and isotropic solids with a cubic lattice ($ax = ay = az$), the α is the same in all directions, and the following expression is valid:

$$\beta = 3\alpha. \quad (3)$$

The Equation (3) is usable for true CTLRs determined at one temperature. The relationship between the volume and linear coefficients obtained over a range of temperatures is more complex [23]:

$$\beta = 3\alpha + 3\alpha^2 t + 3\alpha^3 t^2. \quad (4)$$

However, since the value of α is small, in most cases, for a limited temperature range, a simple relationship between the volumetric and linear coefficients of thermal expansion (Equation (4)) can be adopted with sufficient accuracy.

2. Measurement methods

Studies of the thermal expansion of solids can be carried out using both macroscopic and microscopic methods [24]. Using microscopic (X-ray) methods, the temperature dependence of lattice periods is considered [25–27]. Macroscopic or dilatometric methods examine changes in the volume or length of a sample with temperature. Dilatometers have different operating principles, but their most important characteristic is sensitivity to absolute changes in the dimensions of a body. Optical-mechanical, capacitive, inductive dilatometers are widely used [23, 28–30].

Mechanical dilatometers implement relative measurement of the CTE. In an optical-mechanical dilatometer, the sample expands during heating, displacing the pusher, the movement of which is measured using an optical sensor. In relative dilatometers, it is necessary to have either an intermediate link transmitting the elongation, or a measure relative to which the sample elongation is restrained. The change in the length of the sample is determined either on the basis of preliminary calibration of the device using a reference sample, or from geometric relationships. The main disadvantage of a dilatometer with a pusher is that the results depend on the properties of the reference material.

Thus, an important factor in increasing the measurement accuracy is the choice of the reference material. Standards or reference samples for CTE measurements are selected depending on the technique, the required measurement accuracy, the temperature range of measurements, and the value of the measured CTE. A brief overview of standards is presented in [23]. For example, a standard sample of vitreous silica is used in mechanical dilatometers, which is intended for measuring materials with CTE above $5 \cdot 10^{-6}$ K^{-1} in the range from 144 to 873 K. Quartz allows measurements to be made from 93 to 1173 K. The aluminum oxide and graphite extend the temperature range to 1873 and 2773 K, respectively. For high-precision thermal expansion measurement, especially for materials with CTE less than $5 \cdot 10^{-6}$ K^{-1}, ASTM E 289-2017 [31] describes interferometric methods for solids in the range of 123–973 K with an accuracy of $\pm 0.04 \cdot 10^{-6}$ K^{-1}.

In principle, the reference material can be any substance for which the CTE in the temperature range under study is accurately known. The thermal expansion of the reference material must be reproducible and stable over time at a constant temperature. To avoid errors due to the occurrence of thermal stresses in the sample, the temperature must be the same throughout the sample, and the furnace in which the measurements are carried out must ensure uniformity and stability of the temperature. Sometimes, a material with expansion coefficients close to zero is chosen as a standard, which corresponds to the "absolute" expansion coefficient and allows simplifying the test procedure [29].

Many dilatometers are mounted horizontally, as this ensures better temperature uniformity within the furnace. In these cases, a slight pressing force is applied to the plunger to ensure good contact between the sample and the plungers. This is especially important when measuring during cooling, as there is a risk of contact loss.

When dealing with heterogeneous or anisotropic materials, full-field data (multi-plane displacement) are required for accurate strain measurements. Among the various full-field measurement methods, digital image correlation (DIC) is one of the most popular [28]. It is an optical non-contact experimental method for measuring full-field displacement and strain with sub-pixel accuracy.

There are dilatometers designed to determine the volumetric thermal expansion of melts. However, they are rarely used due to both the choice of a construction material that is resistant to molten salts over a wide temperature range, and the specific design of the dilatometer itself. A vessel made of thin (quartz) glass with a capillary tube, which is the neck of this vessel, is usually used. The tube is equipped with a scale, the graduation of which by the relative change in volume is made by calculation or calibration. In experiments, the change in the volume of the vessel caused by the linear expansion of the vessel material is necessarily taken into account.

Cantor (1969) [32] used a dilatometer, which was a nickel vessel with a narrow neck at the top, to measure the coefficient of volumetric expansion of a molten mixture of fluoride salts. To measure the liquid level, a metal rod was placed in the narrow part of the vessel, which could be moved along the height. The rod was part of an electrical circuit that allowed the liquid level to be measured. The salt was placed in the vessel, heated until it melted, and then the melt level was measured. The

accuracy of the measurements and the sensitivity of such measurements increase with an increase in the ratio of the volumetric expansion coefficients of the melt and the vessel material. If they are equal, this method becomes unsuitable.

Parker (2022) [33] adapted the conventional push-rod dilatometry for the measurement of volumetric expansion of liquid salts using a new graphite crucible design. The efficiency of this method was confirmed by the experimental CTE values of solid and liquid NaCl, which coincided well with the available literature data.

The CTE of molten salts is usually calculated based on the temperature dependence of their density (ρ) or molar volume (V_m), which, in turn, is calculated from the density values using the Equations [34]:

$$\beta = 1/\rho \cdot (\partial\rho/\partial T)_P. \quad (5)$$

$$\beta = 1/V_m \cdot (\partial V_m/\partial T)_P. \quad (6)$$

There are several methods for measuring the density of melts that guarantee high reliability of the experimental values: pycnometric, dilatometric, maximum pressure in a gas bubble, and hydrostatic weighing [35]. Almost all of them are based on the ratio of mass and volume or hydrostatic pressure at fixed external parameters. The main problem in implementing a particular research method is the choice of suitable structural materials resistant to aggressive salt compositions at high temperature. The hydrostatic weighing method based on Archimedes' law is most commonly used to measure the density of molten salts. The principle consists in successive weighing of the load in a gas atmosphere above the melt and in the melt. The load mass change related to its volume is the density of the melt.

Vidrio (2022) [36] performed several series of measurements of the LiF-BeF_2 melt using the classical hydrostatic weighing method and paid much attention to possible sources of error. According to these data, incorrectly prepared mixture composition introduces an error of > 0.6 % per 1 mol. of BeF_2; the amount of impurities in the salt sample from 100 ppm to 1 mol. % introduces an error of about 2 %; non-isothermal measurement conditions - 0.2 %; the presence of dissolved gases in the melt - < 0.3 %; the release of gas bubbles with a change in temperature, depending on the inert gas above the melt - Ar or He, - 0.1 and 0.6 %, respectively. In addition, the measurement error includes the inaccuracy of determining the volume of the load - 0.15 %; weighing error - 0.2 %; melt leakage onto the suspension thread < 0.3 %.

Parker (2022) [37] developed a novel method for density measurement of liquid chlorides by neutron radiography by using a sealed volumetric dilatometer. It is reported that the uncertainty associated with this method is comparable to other techniques.

However, analyzing the literature data, it can be concluded that the most common and reliable method for studying the thermal expansion of molten salts is the calculation of the volumetric expansion coefficient based on the temperature dependence of density, which is usually obtained using the hydrostatic weighing method.

3. Alkali halides

The thermal expansion coefficients of alkali and alkaline earth halides in the temperature range from 0 K to temperatures close to the melting point were studied several decades ago [34, 38, 39]. The main goal of these studies was to create mathematical models based on experimental measurements of thermophysical quantities (thermodynamic expansion coefficient, heat capacity, compressibility, etc.) that explain and predict the thermophysical properties of the material. One of these models, often applied to crystalline salt systems, is the Grüneisen model, which predicts anharmonic properties of the material, such as the coefficient of thermal expansion [24, 40–42].

The Grüneisen parameter (γ) is determined by the change in the frequency of oscillations of the crystal lattice depending on its volume and, as a result, describes the effect of temperature on the size or dynamics of the lattice change. It is usually calculated using an equation that includes experimental quantities: the coefficient of volumetric thermal expansion, the isothermal modulus of bulk compression, the molar volume, and the molar heat capacity at constant volume.

Sunil (2012) [43] calculated the coefficients of volumetric thermal expansion of 16 alkali halides with the NaCl structure, whose crystal lattice consists of ions with a symmetric charge distribution, in the range from room temperature to the melting point, using the Grüneisen model. The RbF has the smallest β (among the 16 halides) ($0.94 \cdot 10^{-4}$ and $1.16 \cdot 10^{-4}$ K^{-1} at 300 and 600 K, respectively), and the LiI has the largest ($1.80 \cdot 10^{-4}$ and $3.02 \cdot 10^{-4}$ K^{-1} at 300 and 600 K, respectively). The alkali fluorides (except RbF) are characterized by similar β values: about $1.2 \cdot 10^{-4}$ K^{-1} at room temperature and $2.05 \cdot 10^{-4}$ K^{-1} at the melting point of the pure salt.

It should be noted that the available experimental CTE values of solids vary according to the different authors, even for the well-studied salt NaCl. The relative deviation of the linear thermal expansion (α) of the solid

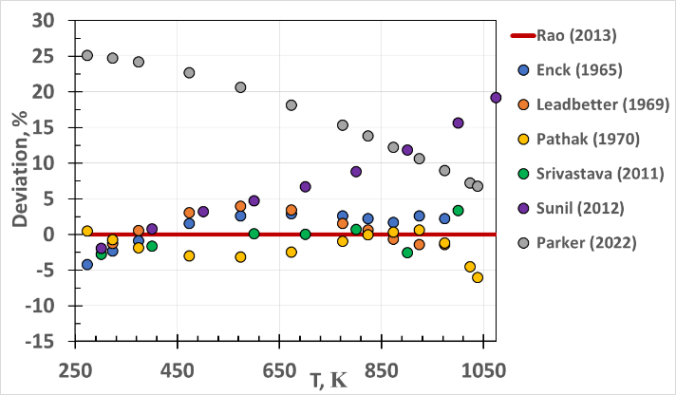

Figure 1 Relative deviations of the linear thermal expansion coefficient (α) of the solid NaCl from the Rao data (2013) [27] obtained in works: Pathak [25], Srivastava [44], Enck [45], Leadbetter [46], Parker [33], Sunil [43].

NaCl from the values obtained by Rao (2013) [27] (by the γ-ray attenuation technique) is presented in Figure 1.

Parker (2022) [33] measured the CTE of the NaCl sample by the conventional push-rod dilatometry. The average value of α $(NaCl)_{solid}$ was reported to be $5.63 \cdot 10^{-5}$ K^{-1} in the temperature range of 300–1050 K.

Pathak (1970) [25] studied the thermal expansion of solid salts by means of a diffractometer. In order to eliminate the temperature gradient in the sample, a special furnace was designed. The X-ray lines were detected by a Geiger counter.

Leadbetter (1969) [46] used a liquid gallium immersion dilatometer, which was constructed of vitreous silica, and the volume change was measured by weighing the gallium expelled through a narrow-bore capillary tube.

Enck (1965) [45] measured the linear thermal expansion for NaCl with an automatic recording dilatometer supplied with the optical system of the interferometric dilation.

Sunil (2012) [43] calculated the thermoelastic properties (thermal expansivity and isothermal bulk modulus) of alkali halides at high temperatures based on the Anderson formula for thermal expansivity and interatomic potential functions within the framework of the Born model.

Srivastava (2011) [44] proposed a model for the estimation of the temperature dependence of the volume expansion ratio and other thermal properties, which was applied to some ionic solids such as NaCl.

As follows from Figure 1, with the exception of the data [33] and [43] obtained by simulation, most of the experimental results agree within ± 5 %.

Another example is the thermal expansion of the solid LiF studied both by experimental methods [47–50] and by modeling [43]. Ekinci (2004) [48] reported new experimental data on the thermal expansion coefficient and the lattice constant of the LiF (0 0 1) surface. The lattice constant was determined from the angular positions of the elastic diffraction peaks observed by in-plane scattering of He atoms. The thermal expansion coefficient was measured with an accuracy of 0.2 %.

Pathak (1972) [47] determined the CTE of solid LiF at different temperatures using a diffractometer, Geiger counter, chart recorder and a specially designed furnace. The CTE temperature dependence was found to be related to the concentration of the thermally generated Schottky defects. The relative deviation of the temperature dependences of the coefficient of linear thermal expansion (α) of solid LiF, obtained by different authors, from the Pathak data [47] are given in Figure 2.

As follows from Figure 2, the values of α coincide within ± 10 % in the temperature range of 273–600 K. At higher temperatures (before melting), the experimental data of Pathak [47] and the calculated data of Sunil [43] are in satisfactory agreement. The values of the coefficient of the LiF linear thermal expansion are $\alpha_{273} = 3.47 \cdot 10^{-5}$ K^{-1}; $\alpha_{673} = 4.58 \cdot 10^{-5}$ K^{-1}; $\alpha_{1173} = 6.96 \cdot 10^{-5}$ K^{-1}.

The temperature dependences of the α for 3 alkali halides (LiF, KCl, CsBr) obtained using the experimental results of the works [25, 47, 51] are presented in Figure 3 in the range from 273 K to temperatures close to the melting point of the salts. It should be noted that an experimental dilatometric determination of the CTE of solid salts cannot be carried out near the melting point. For all the salts shown in Figure 3, the α changes linearly only in the range from 273 K to a certain critical temperature, which is approximately 200 degrees below the melting point: T_m (LiF) = 1121 K, T_m (KCl) = 1043 K, T_m (CsBr) = 909 K. Above the critical temperature, the anomalous part of the thermal expansion may be the result of Schottky defects formed under the influence of

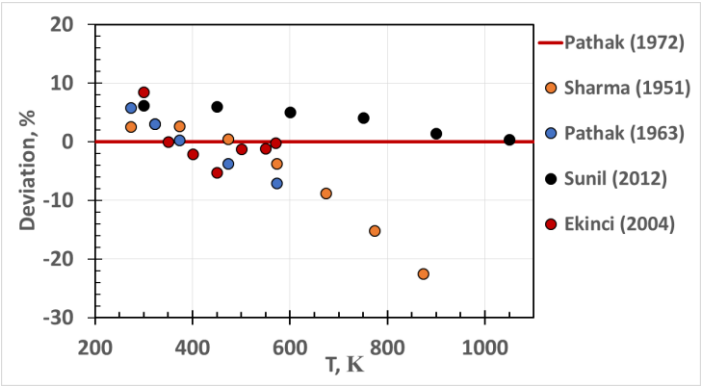

Figure 2 Relative deviations of the linear thermal expansion coefficient (α) of solid LiF from the data of Pathak [47], obtained in the works: Pathak [50], Sharma [49], Sunil [43], Ekinci [48].

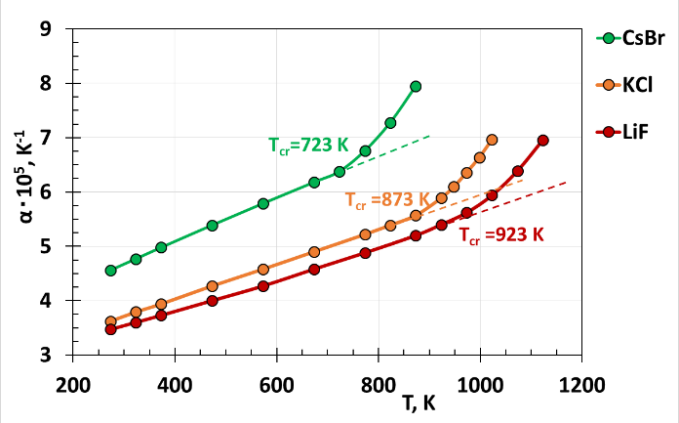

Figure 3 Temperature dependences of the linear thermal expansion coefficient of some alkali halides: LiF [47], KCl [25], CsBr [51], at temperatures not exceeding the melting point of the salts.

high temperatures, which do not play a significant role at lower temperatures [34, 47].

The patterns of change in the thermal expansion of solid salts in the series of halides of one alkali metal can be determined using the example of sodium halides, the temperature dependences of the thermal expansion of which are shown in Figure 4. The experimental values of α for solid NaF, NaCl, NaBr were obtained by Rao (2013) [27], and the calculated values for NaI were borrowed from the publication of Sunil (2012) [43].

It follows from Figure 4 that as the anion size increases, the α rises regularly. As noted above, the thermal expansion temperature dependence of solid alkali halides is nonlinear. However, the linear behavior for NaF is noteworthy. This dependence is described by the Equation:

$$\alpha\,(NaF)_s = 2.5282 + 2.6 \cdot 10^{-3} \cdot T, \qquad (7)$$

with the magnitude of the approximation reliability $R^2 = 0.998$.

However, such a dependence is not observed in a series of salts of the same halogen but with a different cation composition. The α values of solid chlorides and fluorides with different cations according to work [43] are given in Table 1. These are calculated data, but the authors claim a good agreement with the experimental data by Anderson (1995) [52].

If for the alkali fluorides no dependence of α on the cation size is observed, then for the chlorides the opposite trend is found – a decrease in α with an increase in the cation radius. It should be noted that for alkali fluorides and chlorides (except LiCl) the linear expansion coefficients are close in magnitude , their average values ($\alpha_{av.}$) are given in Table 1.

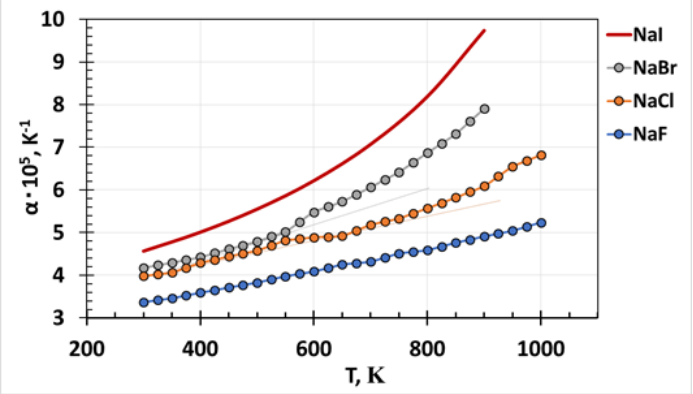

Figure 4 Temperature dependences of the linear thermal expansion coefficient of sodium halides: NaF, NaCl, NaBr [27], NaI [43] at temperatures not exceeding the melting point of the salts.

Table 1 – The linear expansion coefficient ($\alpha \cdot 10^{-5}$ K^{-1}) of alkali chlorides and fluorides at different temperatures [43].

Salt	300 K	600 K	1000 K
LiF	3.33	4.08	6.17
NaF	3.20	3.85	5.52
KF	3.40	4.19	6.43
RbF	3.13	3.88	5.67
$\alpha_{av.}$	3.27 ± 0.13	4.00 ± 0.19	5.95 ± 0.42
LiCl	4.40	6.05	8.06
NaCl	3.97	5.03	6.13
KCl	3.70	4.66	5.70
RbCl	3.43	4.33	5.25
$\alpha_{av.}$ [a]	3.70 ± 0.27	4.67 ± 0.34	5.69 ± 0.44

[a] – α for LiCl was not included in $\alpha_{av.}$.

The maximum deviation of the α from the $\alpha_{av.}$ for fluorides and chlorides (at temperatures up to 600 K) does not exceed 7 %. Thus, the scatter of data and the "reverse" trend of the change in the thermal expansion coefficient with an increase in the cation radius may be associated with errors in the inaccuracy of the initial data for modeling.

The coefficients of volumetric thermal expansion of molten salts are available for almost all alkali halides, since they are easily calculated from the experimental data on the density temperature dependence. As an example, the values of the volumetric thermal expansion coefficient of the molten LiF from various literary sources [53–56] are collected in Table 2.

Table 2 – The volumetric thermal expansion coefficient according to the different authors ($\beta \cdot 10^{-4}$ K^{-1}) of the LiF melt.

T, K	[56]	[53]	[54]	[55]
1150	2.65	1.89	2.58	2.55
1250	2.73	1.93	2.65	2.73

The density data for the molten LiF taken from the handbook by Janz (1968) [56] were obtained by the correlation calculations of all the results available at that time. The authors of [53] and [54] measured the density of the melts by hydrostatic weighing. The most recent data regarding the LiF density were obtained by the gamma-ray attenuation method [55]. The results of [58], [54] and [55] agree within 3 %.

For the molten alkali fluorides and chlorides, the coefficient of volumetric thermal expansion rises as the radius of the cation increases, which is graphically reflected in Figures 5 and 6. The change in β is presented in the temperature range from 300 K to temperatures 100–200 degrees above the melting point. The values of the β for the melts were calculated from the density data given in the reference book [56], for solid salts the β were taken from [43].

As already stated above, the β values of the solid alkali fluorides are close, and for the solid chlorides, a tendency for β to increase as the radius of the cation decreases is clearly traced. In the liquid state for both alkali chlorides and fluorides, the temperature dependence of the volumetric thermal expansion coefficient obeys a linear law and changes slightly with temperature.

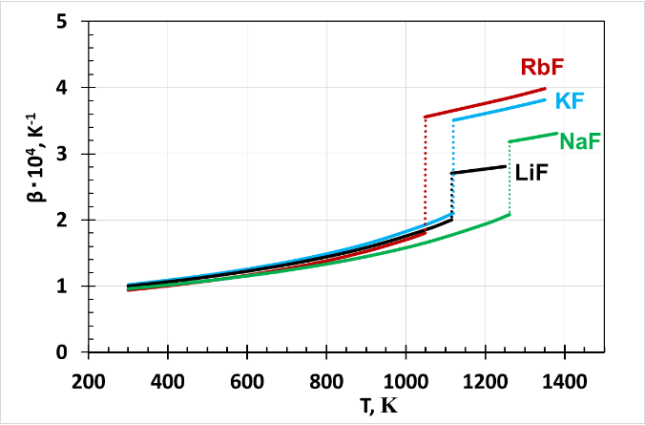

Figure 5 The volumetric thermal expansion coefficient of alkali fluorides. The dotted line indicates the melting point of the salt.

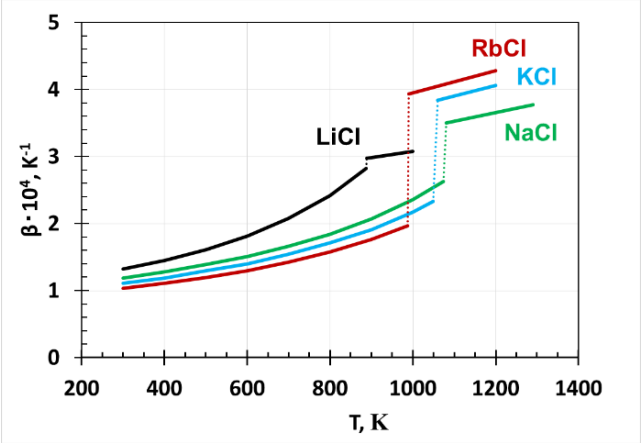

Figure 6 The volumetric thermal expansion coefficient of alkali chlorides. The dotted line indicates the melting point of the salt.

The melting process is accompanied by a jump-like increase in the β. For all salts, the jump in β is greater the larger the size of the alkali cation. It follows from Figures 5 and 6 that the smallest increase in β during melting is observed for LiCl, and β increases almost 2-fold for RbCl.

The properties of molten salts are often considered in terms of their molar volume, which is calculated from the density of the melts. The volume of one mole of each substance contains the same number of particles, equal to Avogadro's number. The molar volume (V_m) depends on the size of the ions, as well as on the interparticle interaction. In the monograph of Minchenko and Stepanov [57], it is noted that the dependence of the alkali halides molar volume on the sum of the cations and anions radii is described by a single linear function. This demonstrates the uniformity of the bond between ions in all alkali halides, which are typical ionic compounds.

The dependence of the volumetric expansion coefficient of alkali halide melts on their molar volume at a temperature of 1300 K is depicted in Figure 7. The density, the coefficient of volumetric expansion and the molar volume of the melts were calculated using the data [57].

The β of all alkali halide melts are practically aligned in a straight line, and their values are greater the greater the molar volume. In general, the volume thermal expansion coefficients of the molten alkali halides vary in the range of $3 \cdot 10^{-4}$–$5 \cdot 10^{-4}$ K^{-1}.

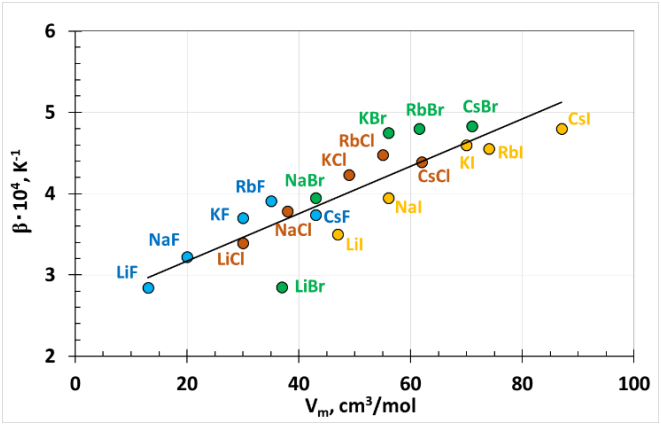

Figure 7 The volumetric thermal expansion coefficient of alkali halide melts depending on their molar volume at 1300 K.

4. Alkaline earth halides

In the series of alkaline earth fluorides, with an increase in the cation size from Ca^{2+} to Sr^{2+} and Ba^{2+}, the

coefficient of linear expansion (α) decreases. Thus, according to the data [34], at room temperature α (CaF_2) = 1.89 · 10^{-5} K^{-1}, α (SrF_2) = 1.81 · 10^{-5} K^{-1}, α (BaF_2) = 1.85 · 10^{-5} K^{-1}.

The experimental data on the temperature dependence of α for the solid alkaline earth halides are scarce. Roberts (1986) [58] measured the α of some solid alkaline earth fluorides and chlorides over a wide temperature range using a dilatometer with an aluminum oxide plunger. The experimental temperature dependences of the coefficient α for the CaF_2, SrF_2, BaF_2, and $SrCl_2$ solid salts are presented in Figure 8.

The coefficients α of the CaF_2, SrF_2 and BaF_2 are close in the range from room temperature to ~ 500 K. They change linearly in the temperature range from 300 K to the critical temperature (in the range of 1100–1200 K), which has a value on average ~ 550 K lower than the melting point of each salt: T_m (CaF_2) = 1691 K, T_m (SrF_2) = 1750 K, T_m (BaF_2) = 1641 K.

The CaF_2, SrF_2 and BaF_2 are characterized by a cubic crystal structure of the fluorite type CaF_2 [59, 60], in which the interatomic distances Me–F are practically identical. The fluorite structure is rather loose, which explains the high mobility of ions with increasing temperature. The authors [58] do not explain the anomalous behavior of α at temperatures above 1100 K, however, they note that the change in the heat capacity of these compounds with temperature has a similar tendency.

The temperature dependence of the coefficient α for solid BeF_2 differs significantly from that of the alkaline earth fluorides of group II*A*. The structure of BeF_2 is a quartz-like tetrahedral network [61–63]. The hexagonal modifications of α-quartz BeF_2 (crystalline SiO_2 structure) and γ-quartz BeF_2 are known, as well as a tetragonal modification of the α-cristobalite type, which at 303 K transforms into a cubic modification of the β-cristobalite type with T_m = 1073 K.

Wright (1988) [62] investigated the phase transformations and crystallographic structure of BeF_2 at temperatures not exceeding the melting point and discovered a significant expansion of the γ-quartz BeF_2 in the temperature range of 303–503 K. The average coefficient of linear thermal expansion along the *c* axis calculated from these data was α_c (BeF_2) = 8.15 · 10^{-5} K^{-1}, and along the *a* axis – α_a (BeF_2) = 6.6 · 10^{-5} K^{-1}. At the same time, a rather large error of these calculations was noted, equal to ± 1.0 · 10^{-5} K^{-1}. Gan (2022) [63] modeled the linear and volumetric thermal expansion coefficients of the α-quartz BeF_2 and α-cristobalite BeF_2. In the temperature range of 300–1500 K, the linear CTEs along

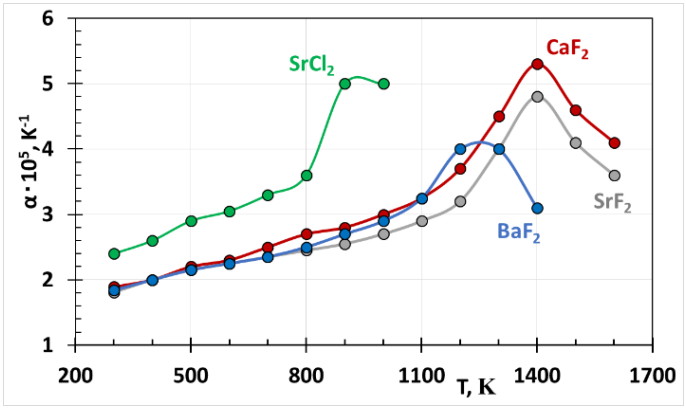

Figure 8 Temperature dependence of the linear thermal expansion coefficient of solid CaF_2, SrF_2, BaF_2, and $SrCl_2$ [58].

both axes have an almost constant value. It should be noted that the solid-liquid phase transition (T_m (BeF_2) = 831 K) is practically not reflected in the model curves of the temperature dependence. Nevertheless, based on these data, it is possible to estimate the value of the volumetric CTE of α-quartz BeF_2, which is ~ 8.0 · 10^{-5} K^{-1} at 300 K and ~ 8.5–9.0 · 10^{-5} K^{-1} at temperatures above 500 K. Accordingly, the linear expansion coefficient of BeF_2 has values from 2 to 3 · 10^{-5} K^{-1} in a wide temperature range.

The change in the volumetric thermal expansion coefficient for the solid and liquid alkaline earth fluorides CaF_2, SrF_2 and BaF_2, as well as for the molten BeF_2 and MgF_2 in a wide temperature range is depicted in Figure 9. The dotted lines connect the β values at the melting temperature with the last experimental points obtained for the solid state [58]. It is not clear what kind of the β temperature dependence exhibits in this range.

The coefficients β of the molten salts MgF_2 and SrF_2 were calculated according to the data of Takeda (2015) [64], and CaF_2 and BaF_2 – according to Kirshenbaum (1960) [65]. For solid MgF_2, the β was not found in the

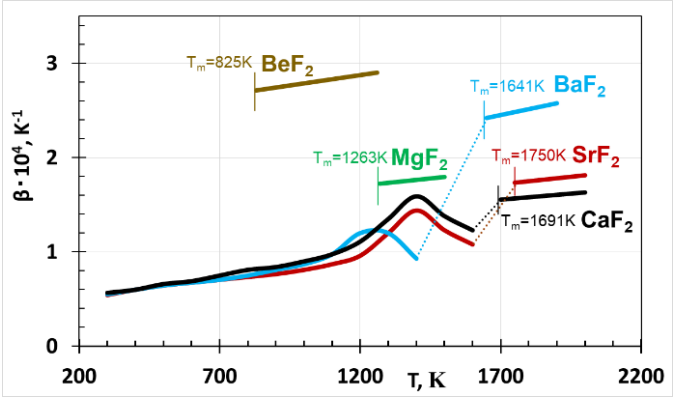

Figure 9 The volumetric thermal expansion coefficient of the solid and liquid fluorides of metals II*A*. The melting points of the salts are marked with vertical lines.

literature in the range from 300 K to temperatures close to the melting point, and there are only model data [63] for the BeF_2. The values of the density of the molten BeF_2 differ significantly according to different sources. The temperature dependence of β (BeF_2) was calculated on the basis of the molten BeF_2 density data obtained by Krylosov (2023) [66]. However, when using the equation from the Janz handbook [56] to calculate β (BeF_2), the value obtained is 4 times greater: β (BeF_2) = $8.07 \cdot 10^{-4}$ K^{-1} at 830 K.

The coefficient β of the liquid alkaline earth fluorides CaF_2, SrF_2 and BaF_2 rises regularly with increasing the cation radius. However, β (BeF_2) and β (MgF_2) do not fit into this sequence, which is explained by significant differences in the structure of their molecules and the type of chemical bonds, and significantly smaller ion radii [57, 67].

Kim (2021) [68] studied the molten structure of MgF_2 using MD simulation and found that MgF_2, which forms an octahedral structure in the solid state, combines one or two fluorine atoms into an octahedral unit of MgF_6 in the molten state and forms a three-dimensional network structure. Li (2023) [69] using molecular dynamics calculated that beryllium ions form chains, that is, BeF_2 is a network system and the so-called "across network interaction mechanism" is also characteristic of BeF_2.

A comparison of the experimental data obtained for SrF_2 and $SrCl_2$, presented in Figure 8, illustrates that the dependence of the coefficient α ($SrCl_2$) on temperature has the same shape as the dependence α (SrF_2) = $f(T)$, however the values for α ($SrCl_2$) are higher than those for α (SrF_2). The temperature dependences of the thermal expansion coefficient for other solid alkaline earth chlorides have not been found in the literature. Nevertheless, it can be assumed that the alkaline earth chlorides in the solid state have higher expansion coefficients than fluorides. This conclusion does not contradict the statement that the coefficient of thermal expansion of salt is higher, the larger the size of the ions.

The β of the molten chlorides of Group II*A* metals, calculated according to Janz (1988) [70], are presented in Table 3 for temperatures 10 degrees above the liquidus of each salt and 1300 K.

It follows from Table 3 that the CTE of chlorides increases with the growth of the cation radius from Mg^{2+} to Ba^{2+}, but β ($BeCl_2$) has a significantly higher value. The dependence of the β for fluorides and chlorides of group II*A* metals on the molar volume is complex and is not described by a linear function, and the β values for beryllium and magnesium salts generally fall outside the overall pattern (Figure 10).

Table 3 – The volumetric thermal expansion coefficients ($\beta \cdot 10^{-4}$ K^{-1}) of molten fluorides of group II*A*.

	$BeCl_2$	$MgCl_2$	$CaCl_2$	$SrCl_2$	$BaCl_2$
$T_{m.p.}$, K	713	987	1056	1145	1230
β ($T_{m.p.}$ + 10) · 10^4, K^{-1}	7.43	1.80	2.04	2.13	2.15
(1300) · 10^4, K^{-1}	13.0	1.91	2.14	2.19	2.17

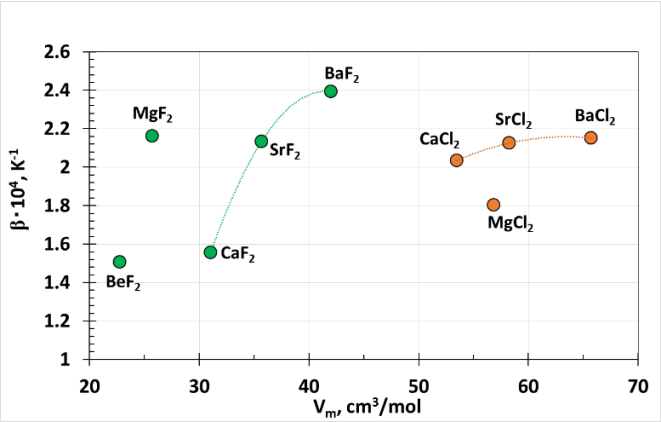

Figure 10 The volumetric thermal expansion coefficient of molten fluorides and chlorides of group II*A* metals depending on their molar volume at temperatures 10 degrees higher than the liquidus temperature of each salt.

The volume of one mole of $MgCl_2$ is larger than the volume of one mole of $CaCl_2$, despite the significantly smaller radius of the magnesium ion. Roy (2021) [71] found by means of computational analysis using five DFT methods that octahedrally coordinated magnesium in solid $MgCl_2$ upon melting is predominantly coordinated with five chloride anions, forming distorted square pyramidal polyhedra $MgCl_5^{3-}$. This species is in equilibrium with four-coordinate $MgCl_4^{2-}$ and six-coordinate $MgCl_6^{4-}$ complexes present as minor components in pure molten $MgCl_2$. According to Bu (2021) [72], with increasing temperature, the typical ionic structure of molten $CaCl_2$ does not change significantly and is an irregularly distorted octahedron, the Cl^- ions around the Ca^{2+} ions are not fixed and are in dynamic equilibrium.

The molar volume of liquid $BeCl_2$ exceeds that of any other alkaline earth halide. Pavlatou (2000) [73] found that two types of polynuclear beryllium ionic species are formed in molten $BeCl_2$, one consisting of a "chain" of edge-bridged $BeCl_4$ tetrahedra and the other having a "cluster" like structure of vertex-bridged $BeCl_4$ tetrahedra.

Thus, for the alkaline earth (Ca, Sr, Ba) fluorides and chlorides melts, the ionic type of interaction is typical,

while the magnesium and beryllium compounds have a complex structure of associated particles.

5. Conclusions

The thermal expansion of solid salts of alkali and alkaline earth halides does not obey a linear law in the range from 300 K to temperatures close to the melting point. This fact can be explained by the significant contribution of defects to the volume of the crystal lattice and a change in the mechanism of increasing interionic distances with increasing temperature.

For solid alkali and alkaline earth (calcium, strontium, barium) fluorides and chlorides, the coefficients of linear expansion are close in value in the temperature range up to the critical point of each salt, and there is no tendency for the CTE to increase upon heating with increasing ion radii. However, this pattern is preserved for molten alkali and alkaline earth fluorides and chlorides. In the liquid state, the temperature dependence of the volumetric thermal expansion coefficient is linear and changes slightly with temperature. When salts melt, the volumetric thermal expansion coefficient increases, and the increase is greater the larger the cation size.

The dependence of the volume expansion coefficients of all molten alkali halides on the molar volume can be described by a linear function, but for alkaline earth fluorides and chlorides such a dependence has a more complex nature. Nevertheless, both dependences indicate the uniformity of interparticle interactions in these salts and the ionic nature of the bond. However, the structure of molten beryllium and magnesium salts is characterized by an intricate structure of complexes, associates of polynuclear ions, chains or clusters. Their thermal expansion does not obey the established regularities.

Supplementary materials

No supplementary materials are available.

Funding

This research had no external funding.

Acknowledgments

None.

Author contributions

Olga Tkacheva: Conceptualization; Data curation; Writing – Original draft; Writing – Review & Editing; Formal Analysis; Software; Visualization.

Conflict of interest

The authors declare no conflict of interest.

Additional information

Author IDs:
Scopus ID: 21733871800;
WoS ResearcherID: D-6844-2017;
ORCID: 0000-0001-5451-2915.

References

1. Tiwari R, Devendra K, Dipendra KV, Parwati K, et al., Fundamental chemical and physical properties of electrolytes in energy storage devices: A review, J. Energy Storage., **81** (2024) 110361. https://doi.org/10.1016/j.est.2023.110361

2. Bo C, Phase change behaviour of some latent heat storage media based on calcium chloride hexahydrate, Solar Energy, **83(4)** (2009) 485–500. https://doi.org/10.1016/j.solener.2008.09.004

3. Tao B, Zhong D, Li H, Wang G, et al., Halide solid-state electrolytes for all-solid-state batteries: structural design, synthesis, environmental stability, interface optimization and challenges, Chem. Sci., **14** (2023) 8693–8722. https://doi.org/10.1039/d3sc02093b

4. Babaev BD, Principles of heat accumulation and heat accumulating materials in use, High Temperature, **52(5)** (2014) 736–751. https://doi.org/10.1134/S0018151X14050010

5. Redkin A, Apisarov A, Dedyukhin A, Kovrov V, et al., Recent developments in low-temperature electrolysis of aluminum, ECS Transactions, **50(11)** (2012) 205–213. https://doi.org/10.1149/05011.0205ecst

6. Zaikov Yu, Batukhtin V, Shurov N, Suzdaltsev A, High-temperature electrochemistry of calcium, Electrochem. Mater. Technol., **1** (2022) 20221007. https://doi.org/10.15826/elmattech.2022.1.007

7. Haarberg GM. Alkali and Alkaline Earth Metal Production by Molten Salt. In: Kreysa G, Ota K, Savinell RF. (eds) Encyclopedia of Applied Electrochemistry. New York, United States: Springer; 2014. p. 21–25. https://doi.org/10.1007/978-1-4419-6996-5_451

8. Wang Z, Cheng Y, He F, Lv Z, Electroplating of refractory metals in molten salts: A Review, JOM, **76(8)** (2024) 4050–4067. https://doi.org/10.1007/s11837-024-06695-z

9. Fache M, Voigt L, Colle JY, Hald J, et al., Thermophysical properties of FUNaK (NaF-KF-UF_4) eutectics, Materials, **17(11)** (2024) 2776. https://doi.org/10.3390/ma17112776

10. Magnusson J, Memmott M, Munro T, Review of thermophysical property methods applied to fueled and un-fueled molten salts, Annals of Nuclear Energy, **146** (2020) 107608. https://doi.org/10.1016/j.anucene.2020.107608

11. Barnes J, Coutts R, Horne T, Thai J, Characterization of molten salt for application in molten salt reactors, PAM Review Energy Science and Technology, **6** (2019) 39–54. https://doi.org/10.5130/pamr.v6i0.1546

12. Mullin KM, Martin JH, Roper CS, Levi CG, et al., Transpiration cooling of a porous Nb-based alloy in high heat flux conditions, Inter. J. Thermal Sci., **196** (2024) 108758. https://doi.org/10.1016/j.ijthermalsci.2023.108758

13. Wood RJK, Lu P, Coatings and surface modification of alloys for tribo-corrosion applications, Coatings, **14(1)** (2024) 99. https://doi.org/10.3390/coatings14010099

14. Ivanova A, Arkhipov P, Tkacheva O, Zaykov Yu, Experimental studies of the dynamic formation of the side ledge in an aluminum electrolysis cell, Russian Metallurgy (Metally), **2** (2020) 133–137. https://doi.org/10.1134/S0036029520020068

15. Tkacheva O, Arkhipov P, Kataev A, Rudenko A, et al., Solid phase formation during aluminium electrolysis, Electrochemistry Communications, **110** (2020) 106624. https://doi.org/10.1016/j.elecom.2019.106624

16. Isakov A, Chernyshev A, Apisarov A, Zaikov Yu, Electrodeposition of alloys from halide melts in solid state, Mater. Technol., **3** (2024) 20243036. https://doi.org/10.15826/elmattech.2024.3.036

17. Sato T, Ohashi K, Sudoh T, Haruna K, et al., Thermal expansion of a high purity synthetic diamond single crystal at low temperatures, Phys. Rev. B, **65** (2002) 092102. https://doi.org/10.1103/PhysRevB.65.092102

18. Bhaduri A. Mechanical Properties and Working of Metals and Alloys. Singapore: Springer Nature Singapore Pte Ltd.; 2018. 748 p. https://doi.org/10.1007/978-981-10-7209-3

19. Nedoseka A. Fundamentals of Evaluation and Diagnostics of Welded Structures. Cambridge, United Kingdom: Cambridge International Science Publishing Limited in association with Woodhead Publishing Limited; 2012. 639 p.

20. Mary TA, Evans JSO, Vogt T, Sleight AW, Negative thermal expansion from 0.3 to 1050 Kelvin in ZrW_2O_8, Science, **272** (1996) 90–92. https://doi.org/10.1126/science.272.5258.90

21. Cahn RW, The how and why of thermal contraction, Nature, **386** (1997) 22–23. https://doi.org/10.1038/386022b0

22. Dubey D, Mirhakimi AS, Elbestawi MA, Negative thermal expansion metamaterials: A review of design, fabrication, and applications, J. Manuf. Mater. Process., **8(1)** (2024) 40. https://doi.org/10.3390/jmmp8010040

23. James JD, Spittle JA, Brown SGR, Evans RW, A review of measurement techniques for the thermal expansion coefficient of metals and alloys at elevated temperatures, Meas. Sci. Technol., **12** (2001) R1–R15. https://doi.org/10.1088/0957-0233/12/3/201

24. Ventura G, Risegari L. The art of cryogenics: low-temperature experimental techniques. Chapter 13. Measurements of thermal expansion. London, UK: Elsevier Ltd.; 2007. p. 289–296. https://doi.org/10.1016/B978-0-08-044479-6.X5001-8

25. Pathak PD, Vasavada NG, Thermal expansion of NaCl, KCl and CsBr by X-ray diffraction and the law of corresponding states, Acta Cryst., **A26** (1970) 655–658. https://doi.org/10.1107/S0567739470001602

26. Hallam KR, Darnbrough JE, Paraskevoulakos C, Peter J, et al., Measurements by X-ray diffraction of the temperature dependence of lattice parameter and crystallite size for isostatically-pressed graphite, Carbon Trends, **4** (2021) 100071. https://doi.org/10.1016/j.cartre.2021.100071

27. Rao ASM, Narender K, Rao KGK, Krishna NG, Thermophysical properties of NaCl, NaBr and NaF by γ–Ray Attenuation Technique, J. Modern Physics, **4** (2013) 208–214. http://dx.doi.org/10.4236/jmp.2013.42029

28. Flament C, Berthel B, Salvia M, at el. Characterization of the thermal behavior of a complex composite (clutch facing) combining digital image stereo correlation and numerical approach, Materials, **15** (2022) 2582–2605. https://doi.org/10.3390/ma15072582

29. Measurement of thermal expansion coefficient using strain gages. Micro-measurements. Vishay Precision Group, Tech. Note TN-513-1, Vishay Measurement Group, Document Number: 11063, (2010) 119–129.

30. Wallace G, Speer W, Ogren J, Es-Said OS, High-resolution methods for measuring the thermal expansion coefficient of aerospace materials, J. Mater. Engineering and Performance, **14** (2005) 563–564. https://doi.org/10.1361/105994905X64602

31. American Society for Testing and Materials. ASTM E289-2017. Standard Test Method for Linear Thermal Expansion of Rigid Solids with Interferometry (2017).

32. Cantor S, Metal dilatometer for determining density and expansivity of volatile liquids at elevated temperature, Rev. Sci. Instrum, **40** (1969) 967–968. https://doi.org/10.1063/1.1684132

33. Parker SS, Abdul-Jabbar NM, Jackson JM, Monreal M, Feasibility of volumetric expansion of molten chlorides by conventional pushrod dilatometry, Radioanal. and Nucl. Chem., **331** (2022) 5259–5263. https://doi.org/10.1007/s10967-022-08641-2

34. Barron THK, Collins JG, White GK, Thermal expansion of solids at low temperatures, Advances in Physics, **29(4)** (1980) 609–730. https://doi.org/10.1080/00018738000101426

35. Park J, Leong A, Zhang J, Density Measurements of Molten Salts, J. Chem. Eng. Data, **68(8)** (2023) 1892–1898. https://doi.org/10.1021/acs.jced.3c00171

36. Vidrio P, Mastromarino S, Still E, et al., Density and thermal expansivity of molten 2LiF-BeF_2 (FLiBe): measurements and uncertainty quantification, J. Chem. Eng. Data, **67** (2022) 3517–3533. https://doi.org/10.1021/acs.jced.2c00212

37. Parker SS, Long A, Lhermitte C, Vogel, et al. Thermophysical properties of liquid chlorides from 600 to 1600 K: Melt point, enthalpy of fusion, and volumetric expansion, J. Mol. Liq., **346** (2022) 118147. https://doi.org/10.1016/j.molliq.2021.118147

38. Cantor S, Ward WT, Moynihant CT, Viscosity and density in molten BeF_2-LiF solutions, J. Chem. Phys., **50(7)** (1969) 2874–2879. https://doi.org/10.1063/1.1671478

39. Yates B, Panter CH, Thermal expansion of alkali halides at low temperatures, Proc. Phys. Soc., **80** (1962) 373–382. https://doi.org/10.1088/0370-1328/80/2/304

40. Sanditov DS, Mantatov VV, Darmaev MV, Sanditov BD, O parametre Gryunayzena kristallov i stekol. [On the Gruneisen parameter of crystals and glasses], Techn. Phys. **79** (2009) 59–62. Russian.

41. Porter LJ, Justo JF, Yip S, The importance of Grüneisen parameters in developing interatomic potentials, J. Applied Physics, **82(11)** (1997) 5378–5385. https://doi.org/10.1063/1.366305

42. Redmond AD, Yates B, The low temperature thermal expansion of thallous chloride and thallous bromide, J. Phys. C: Solid State Phys., **5** (1972) 1589–1603. https://doi.org/10.1088/0022-3719/5/13/009

43. Sunil K, Sharma BS, Thermoelastic properties of alkali halides at high temperatures, Indian journal of pure & applied physics, **50(6)** (2012) 387–397.

44. Srivastava SK, Sinha P, Analysis of thermal expansion of NaCl and KCl crystals, Indian J. Phys., **85** (2011) 1257–1265. https://doi.org/10.1007/s12648-011-0151-2

45. Enck FD, Dommel JG, Behavior of the thermal expansion of NaCl at elevated temperatures, J. Applied Physics, **36(3)** (1965) 839–844. https://doi.org/10.1063/1.1714229

46. Leadbetter AJ, Newsham DMT, Anharmonic effects in the thermodynamic properties of solids. A liquid gallium immersion dilatometer for the range 50–700 °C: thermal expansivities of Hg, Ga, NaCl and KCl, J. Phys. C: Solid State Physics, **2(2)** (1969) 210–219. https://doi.org/10.1088/0022-3719/2/2/303

47. Pathak PD, Vasavada NG, Thermal expansion of LiF by X-ray diffraction and the temperature variation of its frequency spectrum, Acta Crystallographica, **A28** (1972) 30–33. https://doi.org/10.1107/S0567739472000063

48. Ekinci Y, Toennies JP, Thermal expansion of the LiF(001) surface, Science, **563(1–3)** (2004) 127–134. https://doi.org/10.1016/j.susc.2004.06.147

49. Sharma SS, Thermal expansion of crystals, Proc. Indian Acad. Sci. (Math. Sci.), **33** (1951) 283. https://doi.org/10.1007/BF03173262

50. Pathak PD, Pandya NV, Ghadiali MP, Thermal expansion of some alkali fluorides and magnesium oxide by X-ray diffraction, Indian J. Phys., **37** (1963) 293–298.

51. Panter CH, Thermal expansion of caesium bromide and potassium bromide, J. Phys. C: Solid State Physics, **7** (1974) 4483–4485. https://doi.org/10.1088/0022-3719/7/24/010

52. Anderson OL. Equation of state of solids for geophysics and ceramic science, New York, United States: Oxford University Press; 1995. 370 p. https://doi.org/10.1093/oso/9780195056068.001.0001

53. Smirnov MV, Khokhlov VA, Khokhlov VA, et al., Fiziko-khimicheskiye svoystva rasplavlennykh ftoridov shchelochnykh metallov [Physicochemical properties of molten alkali metal fluorides], J. Phys. Chemistry, **48** (1974) 467–469. Russian

54. Chrenková M, Danek V, Silný V, Density of the System LiF–KF–K_2NbF_7, Chem. Papers, **54** (2000) 272–276.

55. Abdullaev RN, Khairulin RA, Stankus SV, Density and thermal expansion of liquid salts LiF and LiF–NaF, Thermoph. And Aeromech., **30** (2023) 133–136. https://doi.org/10.1134/S0869864323010158

56. Janz GJ, Dampier FW, Lakshminarayanan GR, Lorenz PK, et al. Molten Salts: Volume 1, Electrical Conductance, Density, and Viscosity Data. Washington, USA: U.S. Government Printing Office; 1968. 139 p.

57. Minchenko VI, Stepanov VP. Ionnyye rasplavy: uprugiye i kaloricheskiye svoystva [Ionic melts: elastic and caloric properties]. Ekaterinburg: IHTE UB RAS; 2008. 367 p. Russian

58. Roberts RB, White GK, Thermal expansion of fluorites at high temperatures, J. Physics C: Solid State Physics, **19** (1986) 7167–7172. https://doi.org/10.1088/0022-3719/19/36/008

59. Rodnyi PA, Electron-hole and exciton processes in CaF_2, SrF_2, and BaF_2 crystals (Review), Physics of the Solid State, **66** (2024) 155–171. https://doi.org/10.61011/PSS.2024.02.57911.215

60. Ekimova I, Minakova T, Ogneva T, Phisicochemistry of Alkaline-Earth Metals Oxides, Surface Advanced Materials in Technology and Construction, AIP Conf. Proc., **1698** (2016) 060014. http://dx.doi.org/10.1063/1.4937869

61. Ghalsasi P, Ghalsasi PS, Single crystal X-Ray structure of BeF_2: α-quartz, Inorg. Chem, **50(1)** (2011) 86–89. https://doi.org/10.1021/ic101248g

62. Wright AF, Fitch AF, Wright AC, The preparation and structure of the (α- and β-quartz polymorphs of beryllium fluoride, J. Solid State Chem., **73(2)** (1988) 298–304. https://doi.org/10.1016/0022-4596(88)90113-2

63. Gan CK, Al-Sharif AI, Al-Shormanb A, Qteish AA, First-principles investigation of the linear thermal expansion of BeF_2: giant thermal expansion, RSC Adv., **12** (2022) 26588–26595. https://doi.org/10.1039/d2ra04860d

64. Takeda O, Yanagase K, Anbo Y, Aono M, et al., Density measurement of molten alkaline-earth fluorides using archimedean dual-sinker method, Int. J. Thermophys., **36** (2015) 2674–2686. https://doi.org/10.1007/s10765-015-1994-0

65. Kirshenbaum AD, Cahill JA, Stokes CS, The density of molten fluorides in the range of 1600–2500 K, J. Inorg. Nucl. Chem., **15(3–4)** (1960) 297–304. https://doi.org/10.1016/0022-1902(60)80057-7

66. Krylosov AV, Polovov IB, Rebrin OI, Density and electrical conductivity of molten beryllium fluoride–alkali-metal chloride salt mixtures, Russian Metallurgy (Metally), **2** (2023) 229–234. https://doi.org/0.1134/S003602952302012X

67. Gadzhiev SM, Shabanov OM, Magomedova AO, Dzhamalova SA, Limiting electroconductivity and structure of molten chlorides of alkaline-earth metals, Russian J. Electrochem., **39** (2003) 1083–1088. https://doi.org/10.1023/A:1026171420132

68. Kim Y, Kang J, Viscosity of molten MgF_2-LiF-MgO system and structure investigation using classical molecular dynamics simulations, J. Non-Crystalline Solids, **552** (2021) 120377. https://doi.org/10.1016/j.jnoncrysol.2020.120377

69. Li Z, Wu F, Theoretical insight into the structure of molten LiF, BF_2, YF_3 and ThF_4, J. Radioanalytical and Nuclear Chem., **332** (2023) 1163–1170. https://doi.org/10.1007/s10967-023-08780-0

70. Janz GJ. Thermodynamic and Transport Properties for Molten Salts: Correlation Equations for Critically Evaluated Density, Surface Tension, Electrical Conductance, and Viscosity Data, Volume 17. Washington, USA: American Chemical Society and the American Institute of Physics; 1988. 309 p.

71. Roy S, Brehm M, Sharma S, Wu F, et al., Unraveling local structure of molten salts via X-ray scattering, raman spectroscopy, and Ab Initio molecular dynamics, J. Phys. Chem., **125B** (2021) 5971–5982. https://doi.org/10.1021/acs.jpcb.1c03786

72. Bu M, Liang W, Lu G, Yu J, Static and dynamic ionic structure of molten $CaCl_2$ via first-principles molecular dynamics simulations, Ionics, **27** (2021) 771–779. https://doi.org/10.1007/s11581-020-03852-7

73. Pavlatou EA, Papatheodorou GN, Raman spectroscopic study of in the crystalline, glassy and $BeCl_2$ liquid states and of molten mixtures $BeCl_2$–CsCl, Phys. Chem. Chem. Phys., **2** (2000) 1035–1043. https://doi.org/10.1039/A909120C